Fabrication of an Anionic Polythiophene/ Layered Double Hydroxide Ultrathin Film Showing Red Luminescence and Reversible pH Photoresponse

Dongpeng Yan and Jun Lu

State Key Laboratory of Chemical Resource Engineering, Beijing University of Chemical Technology, Beijing 100029, P.R. China

Jing Ma

Institute of Theoretical and Computational Chemistry, Key Laboratory of Mesoscopic Chemistry of MOE, Nanjing University, Nanjing 210093, P.R. China

Min Wei, David G. Evans, and Xue Duan

State Key Laboratory of Chemical Resource Engineering, Beijing University of Chemical Technology, Beijing 100029, P.R. China

Luminescent ordered ultrathin films (UTFs) based on a sulfonated polythiophene (SPT) and Mg–Al-layered double hydroxide (LDH) nanosheets have been fabricated by the layer-by-layer assembly method. UV-visible absorption and fluorescence spectroscopy showed that there was a stepwise and regular growth of the films with increasing number of deposition cycles. XRD, AFM, and SEM showed that the films had a periodic layered structure with a period of ca. *3.0 nm, and that the thickness can be finely controlled within the range* ca. *26–100 nm. The SPT/LDH UTFs show well-defined polarized photoemission with an anisotropy of* ca. *0.3, and they show a reversible luminescence response to changes in pH. Periodic density functional theoretical calculations gave a band energy of 1.85 eV for the SPT/LDH system and showed that the valence electrons of SPT can be confined in the energy wells formed by the LDH monolayers, which effectively inhibits both the nonradiative relaxation and the π–π stacking interaction of the polymer chromophores.* © 2010 American Institute of Chemical Engineers
AIChE J, 57: 1926–1935, 2011
Keywords: polythiophene, layered double hydroxide, polarized red luminescence, pH sensor, periodic density functional theory

Introduction

Luminescent organic polymer materials have been extensively studied for the past 20 years because of their excellent optoelectronic characteristics and potential applications in fields ranging from light-emitting diodes[1] to biology and

chemical sensors.[2] Their low cost, facile processing, and flexibility have also attracted great interest for use in large-scale flat panel display applications. However, some problems must be resolved before such luminescent materials can be commercialized. For instance, the formation of aggregates in the solid state results in emission quenching, or broadening and shifting of the transitions; low thermal and optical stabilities all lead to relatively short service lifetimes. In addition, compared with their green and blue luminescent analogs, red luminescent polymers show rather poor optical properties owing to their low-band gap accompanied by strong nonradiative relaxation and π–π stacking interactions. Recently, the incorporation of guest luminescent molecules into host matrices has received much attention, because the stability of luminescent molecules can be significantly enhanced by virtue of the host–guest interactions (e.g., electrostatic attraction and hydrogen bonding). Moreover, such supramolecular composites also show novel physical and chemical properties which differ from the simple sum of those of their individual counterparts.

Layered double hydroxides (LDHs) are one type of layered solid host matrix. They can be described by the general formula $[M^{II}_{1-x}M^{III}_{x}(OH)_2]^{x+}A^{n-}_{x/n}\cdot yH_2O$; M^{II} and M^{III} are divalent and trivalent metals, respectively, and A^{n-} is a guest anion. LDHs have a number of advantages over other common host solids. Unlike typical zeolite materials, LDHs exhibit swelling behavior and the interlayer spacing can be adjusted based on the size, shape, and the number of the guest anions; unlike most cationic clays, the layer charge density and elemental composition of LDHs can be tuned during the synthesis process, which facilitates fine control over the properties of the host layer. Therefore, LDH materials have attracted considerable interest in both fundamental research and for their practical applications in the areas of functional additives,[3] catalysis,[4] separation processes,[5] and drug delivery.[6] Some photoactive anions, such as perylene,[7] pyrene,[8] rhodamine B,[9] coumarin,[10] and a ruthenium complex[11] have previously been incorporated into LDH systems. The resulting two-dimensional hybrid nanocomposite materials exhibit high-quality photoluminescent properties with improved luminescent efficiency as a result of the host–guest interactions.

However, the incorporation of photofunctional polymers into an LDH matrix is rather difficult and still remains a challenge, owing to the long chain and large size of the polymer molecules.[12] Recently, much attention has focused on the delamination of LDHs to obtain positively charged individual nanosheets as a way of solving this problem. Based on the pioneering work of Sasaki et al.,[13] assembly of such LDH nanosheets and organic polyanions using a layer-by-layer technique has been shown to be a useful way of fabricating a new type of functional hybrid ultrathin films (UTFs) which combine the properties of organic polymers with those of inorganic materials. Therefore, it can be expected that a composite film formed by alternate assembly of positively charged LDH nanosheets and a negatively charged luminescent polymer would exhibit the following advantages: first, the inorganic LDH can offer a confined and stable microenvironment for immobilization of the luminescent guest anions and enhancement of their thermal and optical stability, which meets the needs of solid state light-emission application; second, the introduction of the inert LDH nanosheets can inhibit the π–π stacking interaction and Förster energy transfer between the polymer species, leading

to an improvement in their light-emission efficiency; third, oriented self-emissive polymers in a host matrix often exhibit[14] well polarized light-emission character, and because the LDH with its 2D layered structure is intrinsically anisotropic, a uniaxial 1D luminescent polymer with its transition dipole moment parallel to its long axis[15] should exhibit special anisotropic emission characteristics when incorporated between the layers of an LDH; finally, the film can be fabricated and film thickness can be precisely controlled by simple manipulations, which facilitates large-scale industrial manufacture.
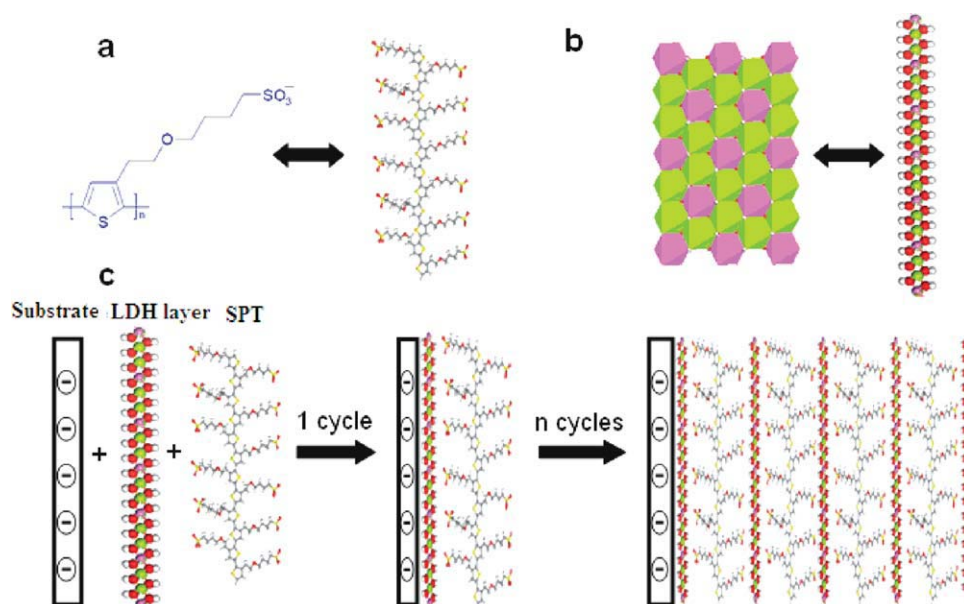
In recent years, because of the rapid increase in computer hardware and software capabilities, much attention has been focused on theoretical calculations as a way of investigating materials at the atomic/molecular scale in many areas of chemical engineering.[16] These theoretical methods provide a complementary tool to experimental procedures for the study and prediction of the structures and properties of new types of functional materials. Unlike classical molecular simulation methods, periodic density functional theoretical (DFT) calculations can be used to study the detailed electronic structures and chemical reactions of atomic systems. DFT has been used to investigate and probe many important properties of both the confined guest molecules and the LDH layers, such as orientation of the guest and the frontier orbitals of the host–guest system. The electronic densities of states for the anions within the LDH galleries (including chloride and hydroxyl anions) have also been studied.[17] To the best of our knowledge, however, most reported DFT studies involved small inorganic anions in the LDH galleries, and very few reports focused on functional anionic species intercalated LDH systems.[18] The detailed understanding of the structural features afforded by DFT calculations would be of great assistance in the design and preparation of materials based on photoactive anions intercalated in LDHs with optimized luminescent properties.

Polythiophene (PT) is one of the most important red-light emitting polymers. Unfortunately, the fluorescence red shifts, broadening, and even luminescence quenching of PT are commonly observed,[19] which restricts its practical applications. Moreover, the sensitivity of PT film materials to pH remains to be investigated. In this work, we report the fabrication of a novel organic–inorganic hybrid UTF system with red luminescence by alternate assembly of a sulfonated polythiophene (SPT) and Mg–Al-LDH nanosheets via the layer-by-layer technique (the assembly process is shown in Scheme 1). The red-light emission, polarization of luminescence, and optical stability under UV irradiation of the hybrid UTF are compared with the pristine SPT film. In addition, the effect of varying the pH on the emission properties of the SPT/LDH UTFs was investigated. Furthermore, the geometric and electronic structures of the SPT/LDH system were investigated by periodic DFT calculations. This work provides a facile method for the fabrication of UTFs with polarized luminescence by incorporation of a photoactive polymer within a 2D inorganic matrix, which can also be used as a pH sensor.

Experimental Section

Reagents and materials

Analytically pure $Mg(NO_3)_2\cdot6H_2O$, $Al(NO_3)_3\cdot9H_2O$ and urea were purchased from Beijing Chemical Co. Ltd. and

Scheme 1. (a) Chemical formula of SPT; (b) Representation of one monolayer of Mg–Al-layered double hydroxide (Mg–Al-LDH) (dark pink: Al(OH)$_6$ octahedra; green: Mg(OH)$_6$ octahedra); (c) the process of assembly of (SPT/LDH)$_n$ UTFs.

[Color figure can be viewed in the online issue, which is available at wileyonlinelibrary.com.]

used without further purification. Sodium poly[2-(3-thienyl)ethoxy-4-butylsulfonate] (SPT, Scheme 1a) was purchased from American Dye Source, Inc.

Fabrication of (SPT/LDH)$_n$ UTFs

The processes of synthesis and exfoliation of Mg–Al-LDH were similar to the procedure described in our previous work.[11] 0.1 g of Mg–Al-LDH was shaken in 100 cm^3 of formamide for 24 h to produce a colloidal suspension of exfoliated Mg–Al-LDH nanosheets. A quartz glass substrate was first cleaned in concentrated NH$_3$/30% H$_2$O$_2$ (7:3) and then concentrated H$_2$SO$_4$ for 30 min in each case. After each step, the quartz substrate was rinsed and washed thoroughly with deionized water. The substrate was dipped in a colloidal suspension (1 g/L) of LDH nanosheets for 10 min followed by thorough washing, and then the substrate was immersed into 100 mL of aqueous SPT solution (0.6 g/L, pH = 7) for 10 min. Multilayer films of (SPT/LDH)$_n$ were fabricated by alternate deposition of the suspension of LDH nanosheets and the SPT solution for n cycles. The resulting films were dried under a nitrogen gas flow for 2 min at 25°C. For the purposes of comparison, drop-cast SPT films were prepared by the solvent evaporation method and were found to show comparable photoluminescence intensity with the (SPT/LDH)$_{32}$ UTF.

Sample characterization

UV-visible absorption spectra were collected in the range 190 to 800 nm on a Shimadzu U-3000 spectrophotometer, with a slit width of 1.0 nm. The fluorescence spectra were recorded on a RF-5301PC spectrofluorophotometer with an excitation wavelength of 437 nm. The fluorescence emission spectra were recorded in the range 450–700 nm, and both the excitation and emission slit were set to 3 nm. The in situ fluorescence measurements of the UV-resistant capability of the film were also per-

formed on the RF-5301PC spectrofluorophotometer. The excitation light source was a 150 W xenon lamp (rated current: 7.5 A; max. current: 8.0 A) with the irradiation wavelength of 360 nm; both the excitation and emission slit were set to 10 nm. In this case, exposure to irradiation of 360 nm can be used to indicate the UV-light resistance ability of the SPT/LDH and drop-cast SPT film, because both of them were detected under the same experimental conditions. Steady-state polarized photoluminescence measurements of SPT/LDH UTFs were recorded with an Edinburgh Instruments FLS 920 spectrofluorimeter. X-ray diffraction patterns (XRD) of SPT/LDH UTFs were recorded using a Rigaku 2500VB2+PC diffractometer under the following conditions: 40 kV, 50 mA, Cu Kα radiation (λ = 0.154056 nm) with step-scanning in steps of 0.04° (2θ) in the range 2 to 12° using a count time of 10 s/step. The morphology of the thin films was investigated by using a scanning electron microscope (SEM Hitachi S-3500) equipped with an EDX attachment (EDX Oxford Instruments Isis 300), with an acceleration voltage of 20 kV. The surface roughness was obtained by using the atomic force microscopy (AFM) software (Digital Instruments, Version 6.12). Electrochemical measurements were carried out with a model 1100A electrochemical analyzer (CH Instruments), using indium tin oxide (ITO) glass as the working electrode, platinum wire as the auxiliary electrode and Ag/Ag$^+$ as the reference electrode. Cyclic voltammetry (CV) studies of the (SPT/LDH)$_n$ (n = 8–32) deposited on ITO glass were carried out in N,N-dimethylformamide solution containing 0.1 M Bu$_4$NBF$_4$ as supporting electrolyte. Using the onset electric potentials in the CV curves, the energy levels of the LUMO (lowest unoccupied molecular orbital) and HOMO (highest occupied molecular orbital) can be determined.

DFT calculations

Detailed construction of the Mg–Al-LDH layer has been fully described elsewhere.[20,21] The lattice parameters were a
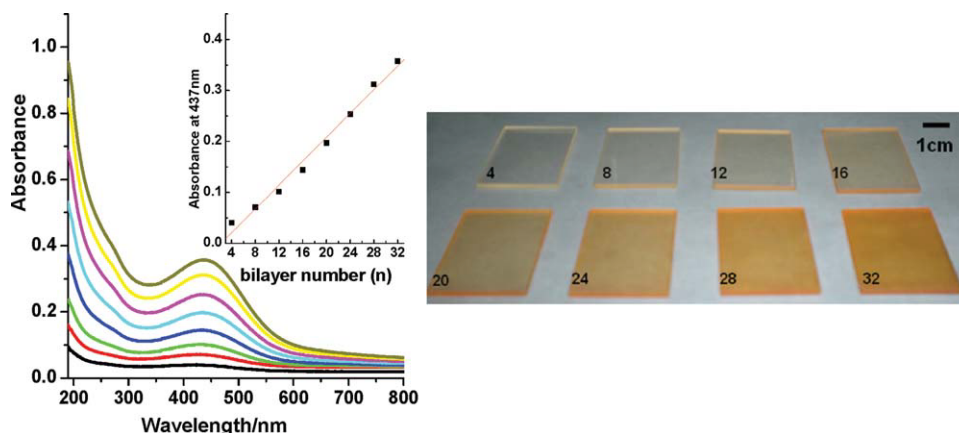
Figure 1. UV/visible absorption spectra of the (SPT/LDH)$_n$ ($n = 4$–32) UTFs (the inset shows the absorbance at 437 nm as a function of the number of bilayers n), and photographs of UTFs with different numbers of bilayers when exposed to daylight.

[Color figure can be viewed in the online issue, which is available at wileyonlinelibrary.com.]

= 18.30 Å, b = 9.15 Å, and the initial basal spacing c = 30 Å (based on the experimental result), $\alpha = \beta = 90°$, $\gamma = 120°$ (equivalent to a $6 \times 3 \times 1$ supercell). The supercell was treated as P1 symmetry, and a three-dimensional periodic boundary condition was applied. Then, a representative oligomer of SPT ($C_{60}H_{80}O_{24}S_{12}$) with six repeat units and six negative charges was introduced into the simulated supercell with the sulfonatopropoxy groups perpendicular to the layers of the LDH. The formula of the simulated structure can be expressed as $Mg_{12}Al_6(OH)_{36}(C_{60}H_{80}O_{24}S_{12})$. All calculations were performed with the periodic DFT method using the DMol^3 module[22] in the Materials Studio software package.[23] The initial configuration was first fully optimized with fixed positions for the atoms in the layer by the classical molecular mechanics method employing the CFF91 force field,[20,21] and further optimization was implemented by the Perdew-Wang (PW91)[24] generalized gradient approximation method with double numerical basis sets plus polarization function (DNP). The core electrons for metals were treated as effective core potentials. The SCF convergence criterion

was within 1.0×10^{-5} hartree/atom and the convergence criterion for structure optimization was 1.0×10^{-3} hartree/bohr. The Brillouin zone (BZ) is sampled by $1 \times 3 \times 1$ k-points since test calculations revealed that an increase in the number of k-points did not affect the results.

Results and Discussion

Fabrication of the SPT/LDH UTFs

Multilayer UTFs were fabricated by alternately dipping a quartz glass slide into a colloidal suspension of LDH nanosheets and an aqueous solution of SPT. The deposition process of the UTFs was monitored by UV-visible absorption spectra after each bilayer cycle as shown in Figure 1. The intensity of the absorption band at *ca.* 437 nm (the π–π* transition of SPT) correlates linearly with n (Figure 1, inset), indicating a stepwise and regular film growth procedure, and this can be further confirmed by the gradual increase in color intensity with increasing number of bilayers (Figure 1). Furthermore, the intensity of the sharp fluorescence peak at *ca.*
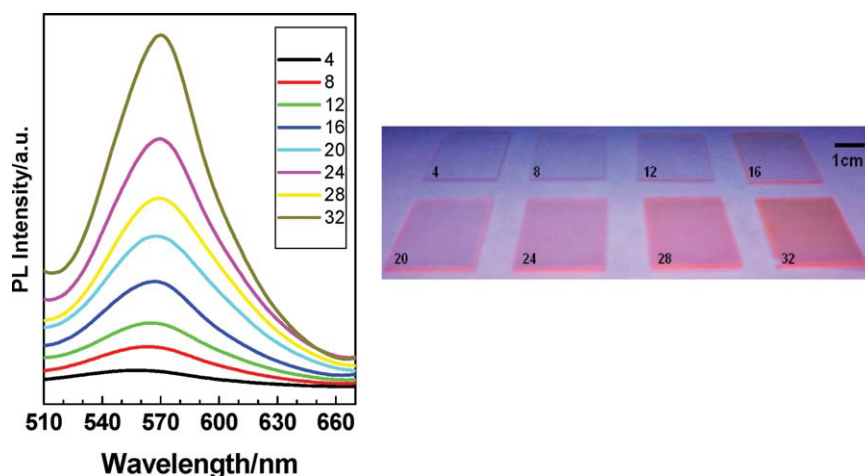

Figure 2. Fluorescence spectra of the (SPT/LDH)$_n$ ($n = 4$–32) UTFs and photographs of UTFs with different numbers of bilayers when exposed to UV light (365 nm).

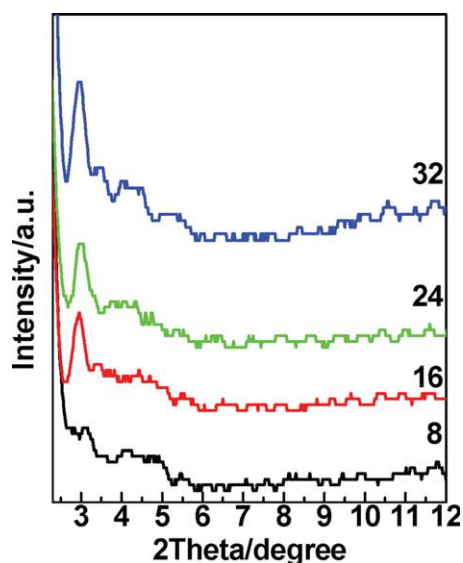[Color figure can be viewed in the online issue, which is available at wileyonlinelibrary.com.]

each other by the rigid LDH nanosheets, which eliminates the possibility of any interlayer π–π stacking interactions.

Characterization of the structure and morphology of the SPT/LDH UTFs

The low-angle XRD patterns of SPT/LDH UTFs are shown in Figure 3. The basal reflection of the as-prepared UTFs appears at *ca.* 2.9–3.2°, and the peak intensity increases with increasing number of bilayers, indicating that the UTF has a periodic long-range ordered structure in the direction normal to the layers with a period thickness of 2.8−3.0 nm. The surface morphology and thickness of SPT/LDH UTFs were investigated by SEM measurements. Typical top-view SEM images of $(SPT/LDH)_n$ UTFs with $n = 8$, 16, 24, and 32 bilayers are displayed in Figure 4, from which it can be seen that the film surface is microscopically smooth and uniform. In addition, by observing the side-view SEM images (the insets in Figure 4), the thickness of films with different numbers of bilayers can be estimated to range from *ca.* 26–100 nm when n increases from 8 to 32. The thickness of the $(SPT/LDH)_n$ UTFs increases linearly as function of the number of deposition cycles, with an average thickness increment of *ca.* 3.0 nm per deposition cycle. Taking into account the thickness of one LDH nanosheet (*ca.* 0.48 nm), the height of the interlayer gallery occupied by the SPT anion along the direction normal to the film is *ca.* 2.5 nm. This value is reasonably consistent with the thickness per bilayer indicated by the side-view SEM images. To obtain quantitative information about the surface roughness of the as-prepared UTFs the $(SPT/LDH)_n$ UTFs were investigated by AFM. The $(SPT/LDH)_8$ UTF had a smooth surface with a root-mean square roughness of 3.03 nm (Figure 5a), and the roughness increased only slightly when increasing n
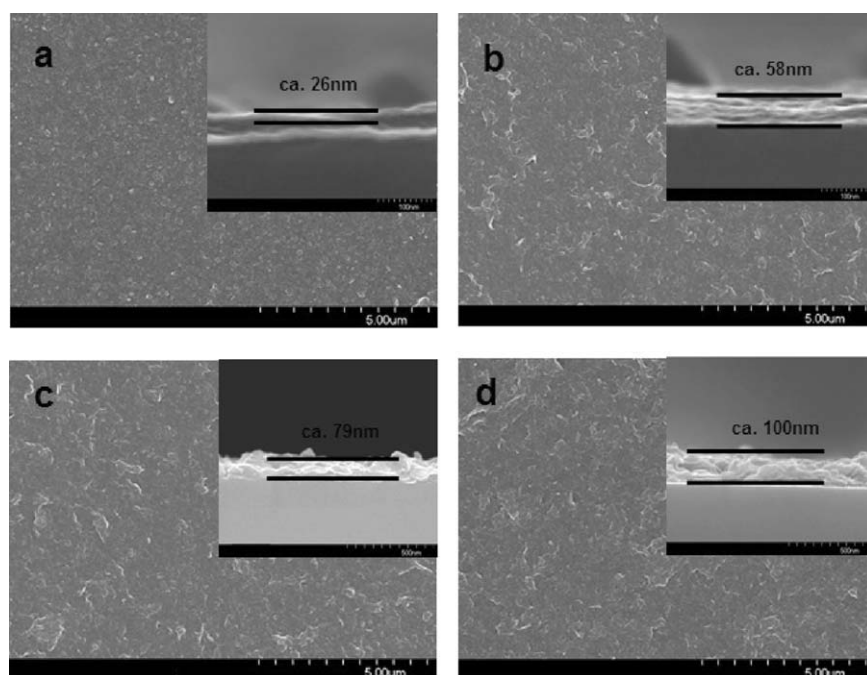

Figure 3. The low angle XRD patterns for the (SPT/LDH)$_n$ UTFs with 8, 16, 24, and 32 bilayers.

[Color figure can be viewed in the online issue, which is available at wileyonlinelibrary.com.]

575 nm of the $(SPT/LDH)_n$ UTFs also displays a consistent increase with n, as shown in Figure 2. Irradiating the thin films with UV light (the inset of Figure 2) also reveals the well-defined red luminescence of the UTFs. The fluorescence spectra of the as-prepared UTFs with different numbers of bilayers show no obvious red or blue shift relative to the spectrum of the pristine SPT solution, demonstrating the absence of SPT aggregates throughout the whole assembly process. This indicates that the polymer chains can be effectively isolated from

Figure 4. SEM images of the (SPT/LDH)$_n$ UTFs in top and side (inset) views for a) $n = 8$; b) $n = 16$; c) $n = 24$; d) $n = 32$.

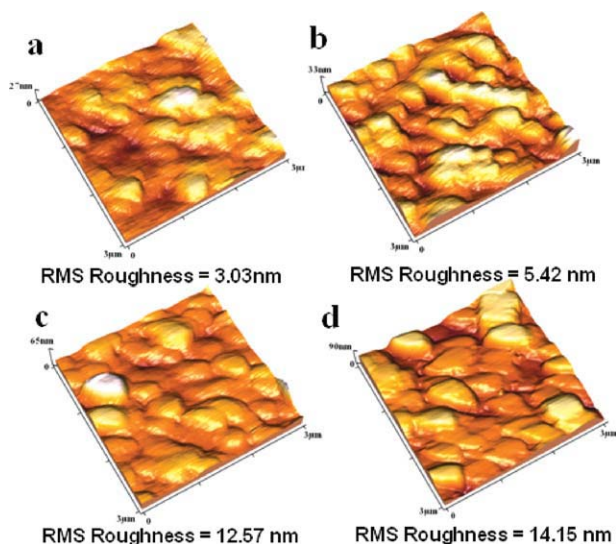**Figure 5. AFM images of the (SPT/LDH)$_n$ UTFs for a) n = 8; b) n = 16; c) n = 24; d) n = 32.**

[Color figure can be viewed in the online issue, which is available at wileyonlinelibrary.com.]

from 16 (5.42 nm) to 32 bilayers (14.15 nm) as shown in Figures 5b–d; the results indicate that all the UTFs are continuous and smooth. AFM image showed that the LDH monolayer was nearly parallel to the UTF surface (Supporting Information Figure S1). The thickness of the monolayer was estimated to be *ca.* 0.57 nm, which is very close to the idealized LDH monolayer (ca. 0.48 nm[9]). Under a fluorescence microscope, all the UTFs show a homogeneous brightness of red color (Figure 6), demonstrating the uniform distribution of SPT chromophores throughout the whole multilayer film.

HOMO and LUMO energies of the SPT/LDH UTFs

CV measurements of the (SPT/LDH)$_n$ UTFs (n = 4−32) were carried out to analyze their electrochemical behavior. It can be seen from Figure 7a that for all the SPT/LDH UTFs, two peaks ($E_{onset,red}$ and $E_{onset,ox}$) were located at *ca.* –0.49 and 1.31 V (vs. Ag/Ag$^+$ electrode), respectively, corresponding to the reduction and oxidation of the electroactive centre
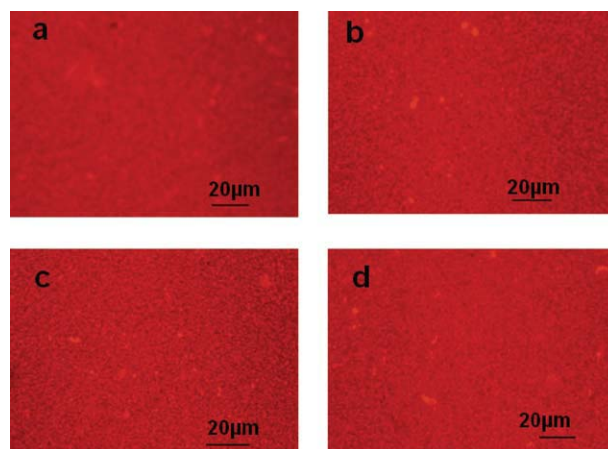

Figure 6. Fluorescence microscope images of the (SPT/LDH)$_n$ UTFs for a) n = 8; b) n = 16; c) n = 24; d) n = 32.

[Color figure can be viewed in the online issue, which is available at wileyonlinelibrary.com.]

of the SPT immobilized between the LDH layers. The peak potentials show no obvious change with varying number of bilayers, suggesting that the oxidation and reduction of SPT were not influenced by the thickness of the UTFs. However, the peak current decreases monotonically with increasing number of bilayers, indicating that the electron transfer was inhibited by increasing film thickness. The effect of varying the scan rate on the electrochemical response of the films is shown in Figure 7b. The anodic and cathodic peak currents were found to be linearly proportional to the square root of the scan rate in the range 0.01 V·s^{-1} to 0.25 V·s^{-1} as shown in the inset of Figure 7b, which is characteristic of a diffusion-controlled process. Based on the empirical relationships proposed by Leeuw et al.,[25] the frontier orbital (HOMO and LUMO) energies can be determined as follows:

$$E(\text{HOMO}) = -(E_{onset,ox} + 4.39) \text{ (eV)}$$
$$E(\text{LUMO}) = -(E_{onset,red} + 4.39) \text{ (eV)}$$

Therefore, the calculated HOMO and LUMO energies of the SPT/LDH UTFs are *ca.* –5.70 and –3.90 eV,
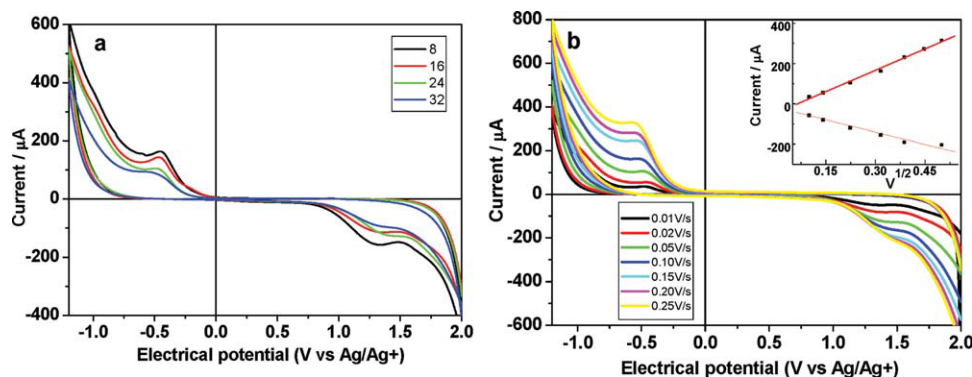

Figure 7. (a) Cyclic voltammograms of the (SPT/LDH)$_n$ UTFs with 8, 16, 24, and 32 bilayers (scan rate: 0.1 V·s^{-1}); (b) Cyclic voltammograms of the (SPT/LDH)$_8$ UTF with different scan rates in the range 0.01 V·s^{-1} to 0.25 V·s^{-1}.

[Color figure can be viewed in the online issue, which is available at wileyonlinelibrary.com.]
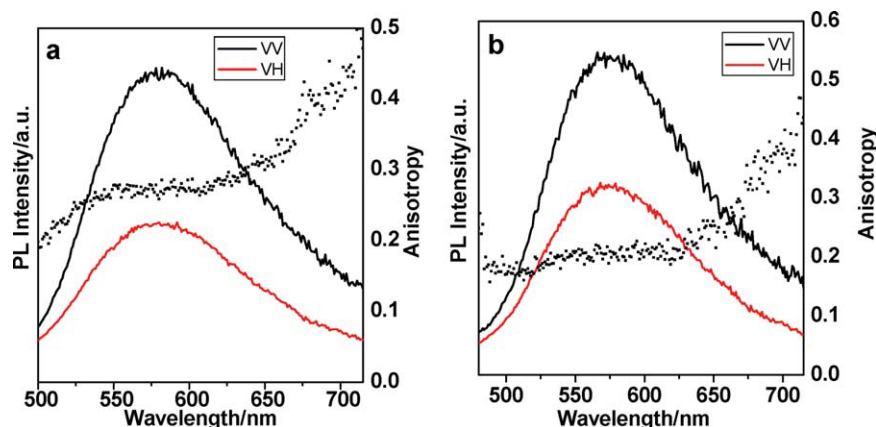
Figure 8. Polarized fluorescence profiles in the VV and VH modes and the anisotropy value (*r*) for the (SPT/LDH)₈ UTF.

a) and b) correspond to excitation light with glancing and normal incidence geometry relative to the UTF, respectively. [Color figure can be viewed in the online issue, which is available at wileyonlinelibrary.com.]

respectively. The calculated band gap energy [$\Delta E_g = E(\text{LUMO}) - E(\text{HOMO})$] is therefore *ca*. 1.8 eV and is essentially independent of the number of assembled bilayers.

Polarized fluorescence of the SPT/LDH UTFs

To further investigate the orientation of SPT polyanions between the LDH nanosheets in the as-prepared UTFs, polarized fluorescence[26] measurements were used to determine the fluorescence anisotropy value *r*. Two typical measurements of polarized fluorescence (glancing and normal incidence geometry) were used to determine the *r* value. The (SPT/LDH)₈ UTF shows a well-defined red fluorescence anisotropy between the parallel and perpendicular directions to the excitation polarization direction (I_{VV} vs. I_{VH}) with an anisotropy value (*r*) of 0.25–0.30 for the in-plane polarized excitation light (Figure 8a); this value is slightly less than the highest value of 0.4 for the system without macroscopic alignment.[22] The I_{VV}/I_{VH} ratio[26] of the glancing incidence measurement is 2.12 at 575 nm, which is larger than that of the vertical excitation and horizontal emission mode by *ca*. 15% (Figure 8b). The uniformity of the *r* value in the range 550−650 nm indicates that polarization scrambling *via* Förster transfer is negligible in the UTFs, and also confirms the rigid-rod and isolated conformation of the SPT chains within the gallery. Furthermore, the *r* value is nearly independent of the number of bilayers in both measurement modes as shown in Supporting Information Figure S2. These results show that the film thickness has no obvious influence on the macroscopic polarized luminescence characteristics of SPT/LDH UTFs, and is indicative of an ordered assembly of the UTFs, which is consistent with the XRD results.

Photostability of the SPT/LDH UTFs

It is interesting to compare the photophysical properties of SPT/LDH UTFs with a pristine SPT film prepared by the drop-casting method. Compared with the SPT/LDH UTFs, the fluorescence peak of the drop-cast SPT film shows a red-shift of *ca*. 25 nm (see Supporting Information Figure S3), which may be induced by π–π interactions of SPT polymer backbones in the latter. To compare the photostability of the two SPT-based films, in situ photoluminescence measurements under continuous UV irradiation were performed for the (SPT/LDH)₃₂ UTF and drop-cast SPT film, because these had very similar initial fluorescence intensities. After irradiation with UV light (360 nm) for 30 min, the fluorescence intensity decreased by *ca*. 21% and 34% for the (SPT/LDH)₃₂ UTF and drop-cast SPT film, respectively (Figure 9, Supporting Information Figure S4). The normalized fluorescence intensity of (SPT/LDH)₃₂ is systematically larger than that of the drop-cast SPT film throughout the whole process (Figure 10). Moreover, the fluorescence intensity of the (SPT/LDH)₃₂ UTF reached a steady value and did not decrease any further after illumination for 20 min, whereas a continuous gradual decrease in intensity with time was observed for the drop-cast SPT film in the range 0−30 min. The results
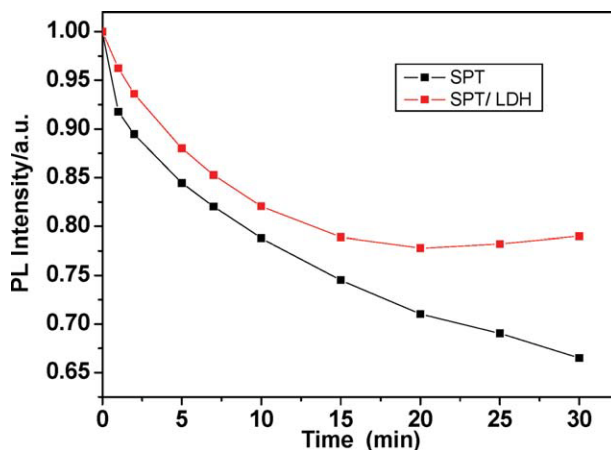

Figure 9. Decay of the normalized maximal PL intensity with irradiation time (360 nm UV light) demonstrating the different UV-resistant capabilities of the (SPT/LDH)₃₂ UTF and the SPT drop-cast film.

[Color figure can be viewed in the online issue, which is available at wileyonlinelibrary.com.]
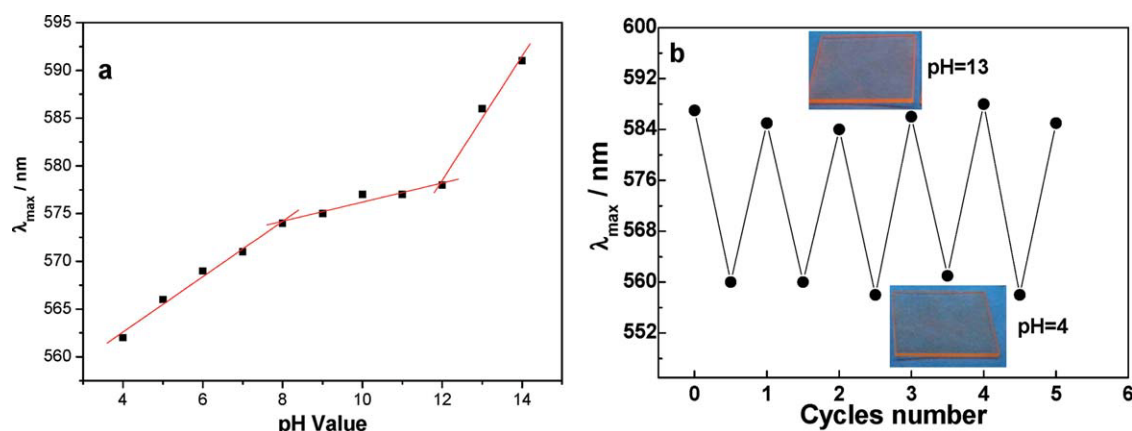
Figure 10. (a) Variation of the maximum photoemission wavelength (λ_{max}) of the (SPT/LDH)$_{32}$ UTF with different pH values; (b) the reversible photoemission response upon alternation between pH = 4 and pH = 13 (the inset show the luminescence photographs of the UTFs at the two pH conditions).

[Color figure can be viewed in the online issue, which is available at wileyonlinelibrary.com.]

demonstrate that the UV-resistance capability of SPT is enhanced significantly by being incorporated with the inorganic LDH nanosheets.

pH-Response behavior of the SPT/LDH UTFs

To investigate the photoemission behaviour of the UTFs under different acid–base conditions, the luminescence spectra of the SPT/LDH UTFs were measured after immersing them in aqueous solutions with pH values varying from 4 to 14 for 10 s (it should be noted that 10 s is a sufficient response time for the proton transfer [see Supporting Information Figure S5]). Figure 10a shows the variation of the maximum emission wavelength of the (SPT/LDH)$_{32}$ UTF with pH, and the photoluminescence spectra are displayed in Supporting Information Figure S6. The dependence of the maximum emission wavelength (λ_{max}) on the pH value can be divided into three main zones: the λ_{max} decreases sharply from 591 to 578 nm (i.e., a blue-shift) as the pH is decreased from 14 to 12; it decreases very slightly from 578 to 574 nm when the pH value decreases from 12 to 8; finally, when the pH value is decreased from 8 to 4, the λ_{max} shows a marked decrease from 574 to 562 nm, which shows a nearly linear relationship with the pH. This sensitivity of the fluorescence performance of the SPT/LDH UTFs to pH can be attributed to the varying extent of protonation and deprotonation of SPT between the LDH nanosheets. The stability and reproducibility of the variation of luminescence properties with pH were explored by repeated alternate immersion of the UTF in aqueous solutions with pH = 4 and pH = 13 (Figure 10b). Typical photographs of the luminescence of the UTF under the two pH conditions are displayed in the inset of Figure 10b, from which it can be observed that the UTF exhibits bright red luminescence at pH = 13 and a relatively dark orange color at pH = 4 under UV illumination. The SPT/LDH UTF shows reversible photoemission response under different pH conditions, indicating its potential application as pH-sensitive luminescence sensor.

Electronic structure calculations

Periodic DFT calculations were carried out for an idealized model of the SPT/LDH structure to further explore its electronic structure. Supporting Information Figure S7 displays the energy band structures of the SPT/LDH system, which exhibits a band gap of *ca.* 1.85 eV at the Γ point (0,0,0) in the first BZ, very close to that of the experimental value (1.80 eV) measured by an electrochemical method. The energy bands around the Fermi level are almost completely independent of the electron wavevector (k) along the ΓZ line (the [001] direction perpendicular to the LDH layer), indicating the strong valence electron confinement effect of the host layer in the normal direction. The greatest valence electron dispersion occurs along the ΓN line (the main chain direction of SPT), suggesting the existence of electron delocalization in the main chain of SPT. In addition, the weak dependence of k on band energy along the ZM line (the direction perpendicular to the main chain of SPT),
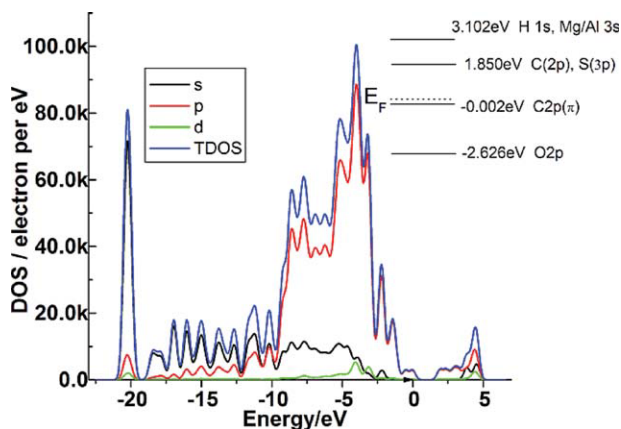

Figure 11. Total and partial electronic densities of state (TDOS and PDOS) for the SPT/LDH system.

The Fermi energy level (E_F) was set as zero. [Color figure can be viewed in the online issue, which is available at wileyonlinelibrary.com.]
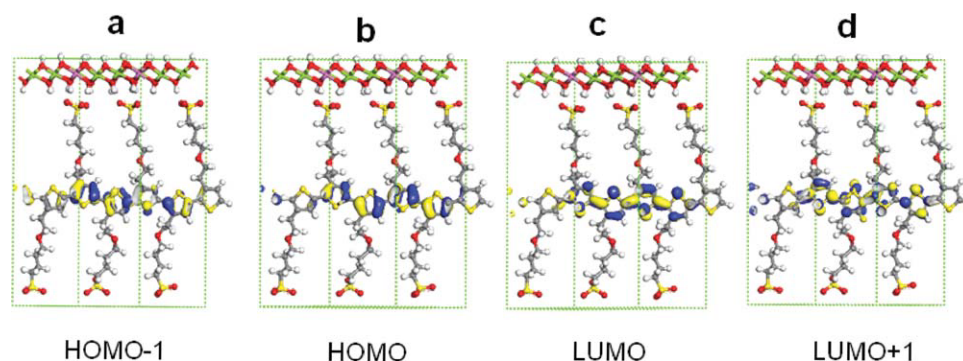
Figure 12. Frontier orbitals (HOMO–1, HOMO, LUMO and LUMO+1) of the DFT-optimized structure of the SPT/LDH system (H white; Al pink; O red; Mg purple; C grey; S yellow; C dark).

[Color figure can be viewed in the online issue, which is available at wileyonlinelibrary.com.]

indicates that the SPT polymers have no significant inter-chain interactions and are dispersed homogeneously in the gallery formed by two LDH monolayers. Figures 11 and 12 present the total electronic densities of states (TDOS) and the frontier orbital profiles of the SPT/LDH system, from which it can be found that the HOMO–1 and HOMO mainly consist of the 2p orbitals of π-conjugated C atoms in the thiophene ring, whereas the LUMO and LUMO+1 are mainly distributed in the 3p orbitals of the S atom and the 2p orbitals of the C atom between the neighboring thiophene rings. Moreover, based on analysis of their partial electronic densities of states (PDOS, Supporting Information Figures S8 and S9), it was found that the O 2p and Mg/Al 3s orbitals in the LDH monolayers contribute to the TDOS below the HOMO, whilst the H 1s orbitals in the LDH monolayers contribute to the TDOS above the LUMO, with a HOMO–LUMO gap of *ca*. 5.7 eV. Around the Fermi level, the TDOS mainly consists of the 2p orbitals of C atoms in SPT. Therefore, the photoexcitation/emission process of the SPT/LDH system mainly occurs in the main chain of the SPT anions, whereas the Mg–Al-LDH monolayers remain inert. This further indicates that the valence electrons localized in the SPT main chains are confined because of the energy blocking effect of the LDH nanosheets. Furthermore, it can be speculated that the SPT/LDH UTF can serve as a multiple quantum well (MQW) structure, which favors stabilization of the valence electronic orbital energies for photoactive polymers, as described in the photostability section.

Conclusion

(SPT/LDH)$_n$ UTFs have been fabricated by a layer-by-layer method and show long-range ordered structures and well-defined red photoluminescence. The assembly of the UTFs can be monitored in detail by UV-visible and fluorescence spectroscopy and XRD. SEM, AFM, and fluorescence microscopy demonstrate that the film surface is microscopically smooth and uniform, and the film thickness correlates linearly with the number of bilayers in the thickness range *ca*. 20 to 100 nm. The presence of LDH monolayers results in an increase in the UV photostability of SPT and the LDH monolayers improve the luminescent properties of SPT by suppressing π–π stacking of the polymer backbones. In addition, the UTFs show well-defined red polarized fluorescence with an anisotropy value of 0.25–0.30. Moreover, the luminescence of the UTFs was shown to be responsive to changes in pH. DFT calculations demonstrated that the SPT/LDH UTF has a relatively low band gap of 1.85 eV. No electron delocalization occurs between SPT and LDH monolayers at the top of valence band, indicating that the LDH monolayer serves as an effective blocking layer and restricts the interlayer interaction of SPT chains, which is consistent with the experimental observations. As a result, the UTF can be regarded as a MQW structure, in which the nonradiative relaxation of the guest is effectively inhibited. Therefore, by virtue of its combination of experimental measurements and theoretical calculations, this work not only gives a detailed description of the luminescent properties, optical stability, and the reversible pH sensitivity of photoactive polymer molecules confined in the LDH host but also provides further understanding of the geometric and electronic structures of MQW host–guest systems. The (SPT/LDH)$_n$ UTFs are prepared by a simple scaleable process and have potential practical applications as a polarized luminescent material and pH-sensitive luminescent sensor.

Literature Cited

1. Burroughs JH, Bradley DDC, Brown AR, Marks RN, Mackay K, Friend RH, Burns PL, Holmes AB. Light-emitting diodes based on conjugated polymers. *Nature*. 1990;347:539–541.
2. Jukka L, Mikko S, Antti V, Timo A, Janika P, Natalia K, Jouko K. Polyelectrolyte multilayers prepared from water-soluble poly(alkoxy-thiophene) derivatives. *J Am Chem Soc*. 2001;123:6083–6091.
3. Evans DG, Duan X. Preparation of layered double hydroxides and their applications as additives in polymers, as precursors to magnetic materials and in biology and medicine. *Chem Commun*. 2006;45:485–496.
4. Wei M, Zhang X, Evans DG, Duan X, Li XJ, Chen H. Rh-TPPTS intercalated layered double hydroxides as hydroformylation catalyst. *AIChE J*. 2007;53:2916–2924.
5. Fogg AM, Dunn JS, Shyu SG, Cary DR, O'Hare D. Selective ion-exchange intercalation of isomeric dicarboxylate anions into the

layered double hydroxide [LiAl$_2$(OH)$_6$]Cl·H$_2$O. *Chem Mater*. 1998;10: 351–355.

6. Zou K, Zhang H, Duan X. Studies on the formation of 5-aminosalicylate intercalated Zn–Al layered double hydroxides as a function of Zn/Al molar ratios and synthesis routes. *Chem Eng Sci*. 2007;62: 2022–2031.

7. Bauer J, Behrens P, Speckbacher M, Langhals H. Composites of perylene chromophores and layered double hydroxides: direct synthesis, characterization, and photo- and chemical stability. *Adv Funct Mater*. 2003;13:241–248.

8. Gago S, Costa T, deMelo JS, Gonçalves IS, Pillinger M. Preparation and photophysical characterization of Zn–Al layered double hydroxides intercalated by anionic pyrene derivatives. *J Mater Chem*. 2008;18:894–904.

9. Yan DP, Lu J, Wei M, Evans DG, Duan X. Sulforhodamine B intercalated layered double hydroxide thin film with polarized photoluminescence. *J Phys Chem B*. 2009;113:1381–1388.

10. Yan DP, Lu J, Ma J, Qin SH, Chen L, Wei M, Evans DG, Duan X. Thin film of coumarin-3-carboxylate and surfactant cointercalated layered double hydroxide with polarized photoluminescence: a joint experimental and molecular dynamics study. *J Mater Chem*. 2010; 20:5016–5024.

11. Yan DP, Lu J, Wei M, Ma J, Evans DG, Duan X. Layer-by-layer assembly of ruthenium (II) complex anion/layered double hydroxide ordered ultrathin films with polarized luminescence. *Chem Commun*. 2009;48:6358–6360.

12. Schöllhorn R. Intercalation systems as nanostructured functional materials. *Chem Mater*. 1996;8:1747–1757.

13. Liu ZP, Ma RZ, Osada M, Iyi N, Ebina Y, Takada K, Sasaki T. Synthesis, anion exchange, and delamination of Co–Al layered double hydroxide: assembly of the exfoliated nanosheet/polyanion composite films and magneto-optical studies. *J Am Chem Soc*. 2006; 128:4872–4880.

14. Nguyen TQ, Wu JJ, Doan V, Schwartz BJ, Tolbert SH. Control of energy transfer in oriented conjugated polymer-mesoporous silica composites. *Science*. 2000;288:652–656.

15. Yoshida Y, Tanigaki N, Yase K, Hotta S. Color-tunable highly polarized emissions from uniaxially aligned thin films of thiophene/ phenylene co-oligomers. *Adv Mater*. 2000;12:1587–1591.

16. Davis ME. The rise and realization of molecular chemical engineering. *AIChE J*. 2009;55:1636–1640.

17. Trave A, Selloni A, Goursot A, Tichit D, Weber J. First principles study of the structure and chemistry of Mg-based hydrotalcite-like anionic clays. *J Phys Chem B*. 2002;106:12291–12296.

18. Cygan RT, Greathouse JA, Heinz H, Kalinichev AG. Molecular models and simulations of layered materials. *J Mater Chem*. 2009; 19:2470–2481.

19. Mattu J, Johansson T, Holdcroft S, Leach GW. Highly ordered polymer films of amphiphilic, regioregular polythiophene derivatives. *J Phys Chem B*. 2006;110:15328–15337.

20. Yan DP, Lu J, Wei M, Li H, Ma J, Li F, Evans DG, Duan X. In situ polymerization of the 4-vinylbenzenesulfonic anion in Ni–Al-layered double hydroxide and its molecular dynamic simulation. *J Phys Chem A*. 2008;112:7671–7681.

21. Yan DP, Lu J, Wei M, Ma J, Evans DG, Duan X. A combined study based on experiment and molecular dynamics: perylene tetracarboxylate intercalated in a layered double hydroxide matrix. *Phys Chem Chem Phys*. 2009;11:9200–9209.

22. Delley B. From molecules to solids with the DMol^3 approach. *J Chem Phys*. 2000;113:7756–7764.

23. *DMol^3 Module, MS Modeling, Version 2.2*. San Diego, CA: Accelrys Inc., 2003.

24. Perdew JP, Chevary JA, Vosko SH, Jackson KA, Pederson MR, Singh DJ, Fiolhais C. Atoms, molecules, solids, and surfaces: applications of the generalized gradient approximation for exchange and correlation. *Phys Rev B*. 1992;46:6671–6687.

25. deLeeuw DM, Simenon MMJ, Brown AR, Einerhand REF. Stability of n-type doped conducting polymers and consequences for polymeric microelectronic devices. *Synth Met*. 1997;87:53–59.

26. Valeur B. Molecular Fluorescence: principles and Applications. Wiley-VCH, Verlag GmbH, 2001. $r = (I_{vv} - GI_{VH})/(I_{vv} + 2GI_{VH})$, where $G = I_{HV}/I_{HH}$, determined using the aqueous solution of SPT. I_{VH} stands for the photoluminescence intensity (I) obtained with *vertical* (V) excitation polarization and *horizontal* (H) detection polarization, and I_{VH}, I_{HV}, I_{HH} are defined in a similar way.